Report

Current Biology

A Population of Interneurons Signals Changes in the Basal Concentration of Serotonin and Mediates Gain Control in the *Drosophila* Antennal Lobe

Graphical Abstract

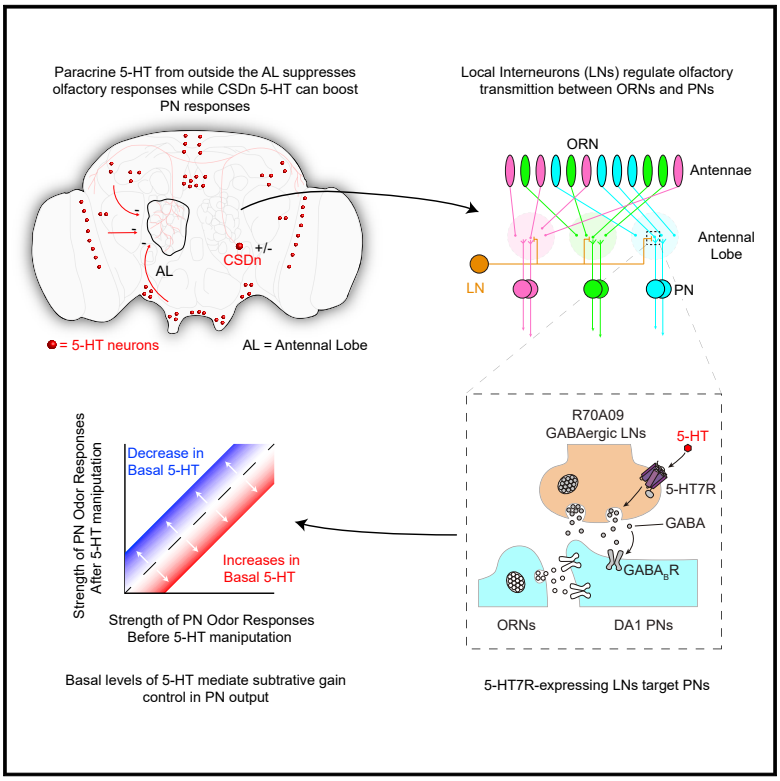

Highlights

- LNs in the *Drosophila* antennal lobe signal changes in basal levels of 5-HT
- Basal levels of 5-HT are detected with the high-affinity 5-HT7 receptor
- 5-HT7R-expressing LNs target PNs for postsynaptic inhibition via GABA
- Low concentrations of 5-HT impart a subtractive gain control on PN output

Authors

Yoshinori Suzuki, Jonathan E. Schenk, Hua Tan, Quentin Gaudry

Correspondence

qgaudry@umd.edu

In Brief

Suzuki et al. identify a population of GABAergic local interneurons responsible for detecting paracrine serotonin in the fly antennal lobe. These interneurons exclusively express the 5-HT7 receptor and target projection neurons for postsynaptic inhibition. This inhibition mediates a subtractive form of gain control on projection neuron output.

Suzuki et al., 2020, Current Biology *30*, 1110–1118
March 23, 2020
https://doi.org/10.1016/j.cub.2020.01.018

CellPress

CellPress

Current Biology
Report

A Population of Interneurons Signals Changes in the Basal Concentration of Serotonin and Mediates Gain Control in the *Drosophila* Antennal Lobe

Yoshinori Suzuki,[1,2] Jonathan E. Schenk,[1,2] Hua Tan,[1] and Quentin Gaudry[1,3,*]
[1]Department of Biology, University of Maryland, College Park, MD 20742, USA
[2]These authors contributed equally
[3]Lead Contact
*Correspondence: qgaudry@umd.edu
https://doi.org/10.1016/j.cub.2020.01.018

SUMMARY

Serotonin (5-HT) represents a quintessential neuromodulator, having been identified in nearly all animal species [1] where it functions in cognition [2], motor control [3], and sensory processing [4]. In the olfactory circuits of flies and mice, serotonin indirectly inhibits odor responses in olfactory receptor neurons (ORNs) via GABAergic local interneurons (LNs) [5, 6]. However, the effects of 5-HT in olfaction are likely complicated, because multiple receptor subtypes are distributed throughout the olfactory bulb (OB) and antennal lobe (AL), the first layers of olfactory neuropil in mammals and insects, respectively [7]. For example, serotonin has a non-monotonic effect on odor responses in *Drosophila* projection neurons (PNs), where low concentrations suppress odor-evoked activity and higher concentrations boost PN responses [8]. Serotonin reaches the AL via the diffusion of paracrine 5-HT through the fly hemolymph [8] and by activation of the contralaterally projecting serotonin-immunoreactive deuterocerebral interneurons (CSDns): the only serotonergic cells that innervate the AL [9, 10]. Concentration-dependent effects could arise by either the expression of multiple 5-HT receptors (5-HTRs) on the same cells or by populations of neurons dedicated to detecting serotonin at different concentrations. Here, we identify a population of LNs that express 5-HT7Rs exclusively to detect basal concentrations of 5-HT. These LNs inhibit PNs via $GABA_B$ receptors and mediate subtractive gain control. LNs expressing 5-HT7Rs are broadly tuned to odors and target every glomerulus in the antennal lobe. Our results demonstrate that serotonergic modulation at low concentrations targets a specific population of LNs to globally downregulate PN odor responses in the AL.

RESULTS

The Effects of Basal Concentrations of 5-HT Are Mediated via the 5-HT7 Receptor

We initially focused on the pheromone-sensitive glomerulus DA1 as those projection neurons (PNs) can be easily targeted using the Q/QUAS binary expression system, thus allowing us to use the Gal4/upstream activating sequence (UAS) system to later manipulate serotonergic transmission. We began by replicating previous results demonstrating that the broad 5-HT receptor (5-HTR) antagonist methysergide boosts responses in PNs *in vivo*. Blocking the *Drosophila* serotonin reuptake transporter (dSerT) with fluoxetine elevates 5-HT at release sites and reduces PN odor responses [8] (Figures 1A–1C). These results suggest a suppressive role for 5-HT on PN output at low concentrations, as both manipulations influence the detection or clearance of 5-HT at basal levels. Although the contralaterally projecting serotonin-immunoreactive deuterocerebral interneurons (CSDns) likely contribute to establishing the basal levels of 5-HT in the antennal lobe (AL), paracrine 5-HT circulating through the hemolymph is also likely involved, as intact CSDns are not required for methysergide's effects on PN responses [8] (Figures S1A–S1H). Whereas manipulating basal concentrations of 5-HT suppresses PN responses, high concentrations of exogenous 5-HT [5, 8] and direct stimulation of the CSDn boosts PN output (Figures S1I–S1L).

We performed a screen to determine specifically which of the five *Drosophila* 5-HTR subtypes are responsible for the effects of 5-HT at basal concentrations. Antagonists against each 5-HTR were tested for their ability to both mimic and occlude methysergide's effect (Figures 1D–1M). Only the 5-HT7R antagonist SB258719 boosted odor activity and prevented methysergide from further elevating DA1 PN responses (Figures 1L and 1M). We used the Gal4/UAS system to express 5-HT7R in DA1 PNs to validate that these reagents indeed antagonize 5-HT7R in *Drosophila*. UV uncaging of 5-HT in control flies without the exogenous receptor indicated that DA1 PNs likely do not express any 5-HTRs (Figure 1N), although including the transgene demonstrated that our antagonists are effective against 5-HT7R (Figures 1N and 1O). Thus, our antagonist screen implicates excitatory 5-HT7Rs as mediating the effects of low or basal concentrations of 5-HT on PN output.

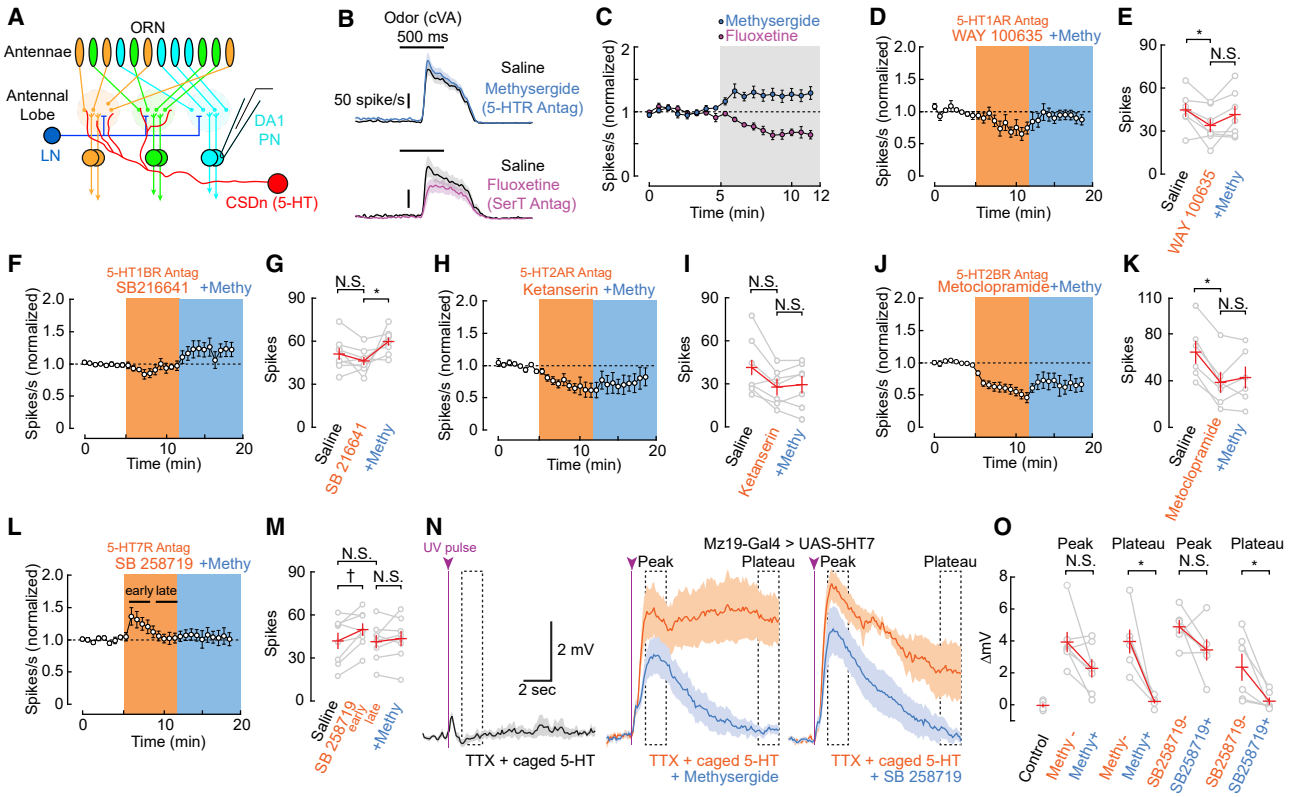

Figure 1. The *Drosophila* 5-HT7R Mediates the Suppression of Odor Responses at Low Concentrations of Serotonin

(A) A schematic of the *Drosophila* antennal lobe showing relevant neurons and connections. Olfactory receptor neurons (ORNs) make feedforward connections onto the dendrites of projection neurons (PNs) in olfactory glomeruli (light colored circles in AL). ORNs expressing the same olfactory receptor are colored identically and project to the same individual glomerulus. GABAergic local interneurons (dark blue) allow communication between glomeruli and participate in various forms of lateral and intra-glomerular inhibition. The AL receives all of its direct serotonergic innervation from a pair of neurons termed the CSDns (red) that innervate nearly all glomeruli, excluding pheromone-sensitive glomeruli, such as DA1. Serotonin can also enter the AL via paracrine sources. See also Figure S1. All recordings in this figure were made from DA1 PNs.

(B) The mean and SEM of peristimulus time histograms (PSTHs) of DA1 PN responses to 11-cis-vaccenyl acetate (cVA) in saline and after the application of 50 μM methysergide (used throughout the study) or 10 μM fluoxetine. Methysergide is a broad 5-HTR antagonist. Fluoxetine raises 5-HT levels by blocking the serotonin transporter, SerT. Whole-cell recordings were made *in vivo* from DA1 PNs labeled with GFP. The horizontal bar above the PSTH indicates the odor stimulus period and serves as scale bar for time (500 ms). This presentation is used throughout subsequent figures. The vertical bar indicates 50 spikes per second.

(C) A time series showing boosting of PN responses by methysergide and suppression by fluoxetine (n = 8 methysergide, p = 0.007, and n = 6 fluoxetine, p = 0.031). All comparisons, including subsequent panels, were performed with a Wilcoxon signed-rank test. Data are normalized to the mean of the response prior to drug application. Error bars indicate ± SEM throughout applicable panels.

(D) Time series of the effects of the 5-HT1AR antagonist WAY100635 and with subsequent application of methysergide.

(E) Quantification of the preceding experiment. n = 7; saline versus drug p = 0.047; drug versus methysergide p = 0.15. N.S., not significant. Mean and SEM are represented by a + thoughout subsequent panels.

(F and G) An identical protocol was used as in (D) and (E) but for the 5-HT1BR antagonist SB216641. n = 8; saline versus drug p = 0.23; drug versus methysergide p = 0.016.

(H and I) As in (D) and (E) but for the 5-HT2AR antagonist ketanserin. n = 7; saline versus drug p = 0.11; drug versus methysergide p = 0.94.

(J and K) As in (D) and (E) but for the 5-HT2BR antagonist metoclopramide. n = 6; saline versus drug p = 0.031; drug versus methysergide p = 0.68.

(L and M) As in (D) and (E) but for the 5-HT7R antagonist SB258719. n = 8; saline versus drug early p = 0.05 (†); saline versus drug late p = 0.84; drug versus methysergide p = 0.74.

(N) Left: control experiment in which 5-HT is photo-uncaged using UV light while recording whole cell from a DA1 PN in saline with TTX. Uncaging 5-HT has no detectable effect on the PNs, suggesting they do not express 5-HTRs. Middle: the 5-HT7R was expressed in DA1 PNs by Gal4/UAS, resulting in their depolarization upon UV-photo-uncaging of 5-HT. The depolarization was effectively blocked by methysergide. Right: SB258719 also effectively blocked the effects of 5-HT at the 5-HT7R.

(O) Quantification of the results in (N). We calculated mean membrane potentials from 1 and 10 s after UV stimulus over 1.5 s as peak and plateau responses, respectively. From left to right, n = 5, 7, 6, 6, and 6; Wilcoxon signed-rank test (p = 0.071; p = 0.031; p = 0.218; p = 0.031).

GABAergic LNs in the AL Enable Sensitivity to Low Concentrations of 5-HT

We next sought to identify which cell classes in the AL express 5-HT7R and may thus mediate the boosting of PNs in response to basal 5-HT levels. Currently, there are no validated antibodies available for *Drosophila* 5-HTRs. Therefore, we used previously described 5-HTR MiMIC GAL4 protein-trap and gene-trap transgenic lines [11–13] and determined their overlap with promoter

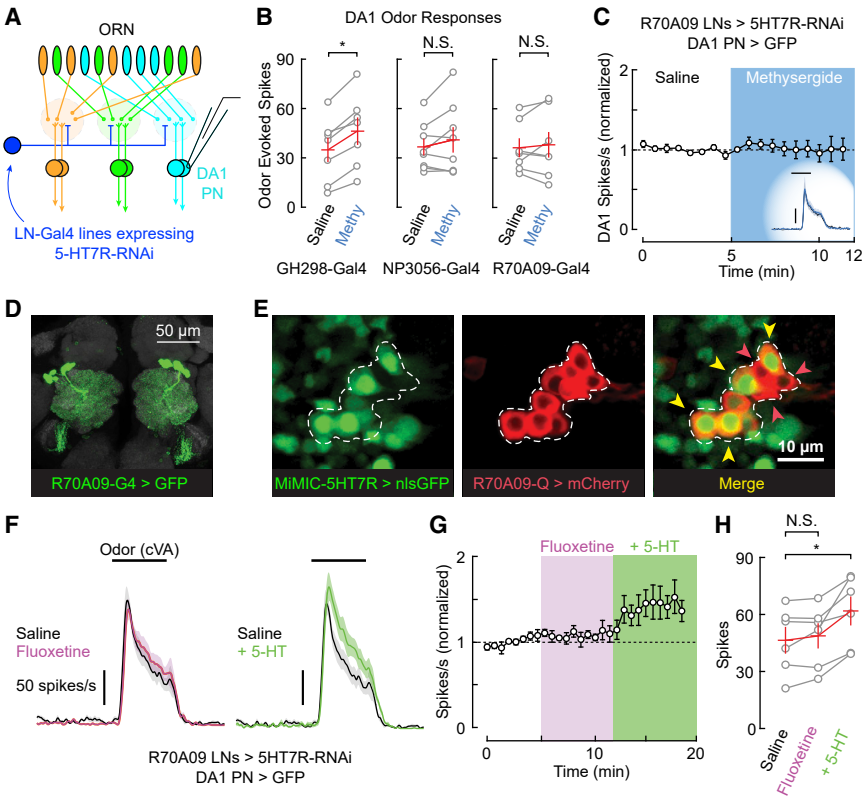

Figure 2. R70A09-Gal4 LNs Express 5-HT7Rs to Detect and Signal Low, but Not High, Concentrations of 5-HT

(A) A schematic of the *Drosophila* olfactory system showing the experimental configuration. Gal4 promoter lines were used to express RNAi against the 5-HT7R in various populations of LNs. The QUAS system was used to express GFP in DA1 PNs for whole-cell recordings. See also Figure S2.

(B) An RNAi against the 5-HT7R was expressed in three LN lines and tested for its ability to block the effects of methysergide. The expression of the construct in the GH298 LN line did not block the effects of methysergide. Expression in both NP3056 and R70A09 did occlude the effects of methysergide. From left to right, n = 7, 8, and 7; Wilcoxon sign-ranked test ($p = 0.015$; $p = 0.64$; $p = 0.812$). Error bars represent SEM.

(C) A time series of DA1 responses from the experiment in (B). Blue shading shows time and duration of methysergide application. Inset: a PSTH of DA1 responses when the 5-HT7R-RNAi is expressed in R70A09 LNs is shown. Horizontal black bar represents the 500-ms odor presentation. The vertical bar indicates 50 spikes per second. The black trace is the mean of the odor responses in saline, and the blue trace is the mean odor response in methysergide.

(D) The R70A09-Gal4 line expresses exclusively in approximately 12 LNs per hemisphere in the AL. See also Figure S3.

(E) The MiMIC-5-HT7 protein trap and the R70A09-Q promoter lines have extensive overlap. 9.3 ± 1.0 R70A09 cells overlap with the 11.25 ± 0.69 LNs of the MiMIC line [12]; replicated in 6 flies.

(F) PSTHs of DA1 odor responses in fluoxetine and exogenous 5-HT. The 5-HT7R-RNAi was expressed in R70A09 LNs via the Gal4/UAS, and DA1 PNs were targeted with Q/QUAS and GFP.

(G) A time series of the odor responses in fluoxetine and subsequently 5-HT.

(H) Quantification of the previous experiments. n = 6; Wilcoxon signed-rank test ($p = 0.56$; $p = 0.03$). Error bars represent SEM.

lines labeling various cell classes in the AL [14, 15]. Consistent with our uncaging experiments, we found no overlap between DA1 PNs and each of the five MiMIC 5-HTR lines (Figures S2A–S2E). This suggests that DA1 PNs are not the direct target of 5-HT7R modulation. Previous studies have shown that olfactory receptor neurons (ORNs) as a population do not express 5-HT7R and may only express 5-HT2BR [12]. We confirmed that the cognate ORNs to the DA1 glomerulus (OR67d ORNs) do express 5-HT2BR (Figures S2F–S2O). Blocking 5-HT2BRs failed to modulate odor responses in OR67d axons in the AL as revealed by GCaMP imaging, suggesting 5-HT2BR is not involved in signaling low basal levels of 5-HT (Figures S2P–S2R). Combined, these results suggest that neither ORNs nor PNs are the likely direct target of 5-HT7R-mediated modulation and thus implicate local interneurons (LNs) as a possible target.

We next expressed an RNAi against 5-HT7R in various Gal4 promoter lines to identify LNs that mediate signaling of basal 5-HT levels in the AL (Figure 2A). Because the effects of SB258719 were more transient, we utilized methysergide and assessed whether knocking down 5-HT7R in each promoter line could prevent the antagonist from boosting DA1 odor responses (Figures 2B and 2C). The GH298-Gal4 and NP3056-Gal4 promoter lines both express broadly within the AL but have no overlap in their expression patterns [15]. We also screened the Janelia FlyLight collection [16] for Gal4 lines generated from fragments of the 5-HT7R promoter and identified R70A09-Gal4, whose AL expression pattern was limited to 12 LNs per hemisphere (Figure 2D). Expression of the 5-HT7R-RNAi in either NP3056 or R70A09 blocks the effects of methysergide (Figures 2B and 2C). Interestingly, NP3056 and R70A09 have little overlap in their expression patterns, suggesting that both populations of LNs must express functional 5-HT7Rs to block the effects of the antagonist and low-concentration 5-HT signaling. We converted R70A09-Gal4 into a Q-system promoter line [17] using the HACK method [18] in order to test for overlap between the R70A09 and the MiMIC 5-HT7R line. The new R70A09-Q promoter line showed 100% overlap with its Gal4 counterpart (Figure S3C), and most R70A09-Q LNs are labeled in the MiMIC 5-HT7R protein trap line, suggesting they indeed express the receptor (Figure 2E).

If R70A09 LNs use 5-HT7Rs to detect low levels of serotonin, then expressing 5-HT7R-RNAi in these cells should also prevent the modulation of DA1 PNs to the serotonin transporter blocker, fluoxetine. Fluoxetine typically suppresses odor responses (Figures 1B and 1C) but failed to do so when 5-HT7Rs were knocked down in R70A09 LNs (Figures 2F–2H). Because serotonin can

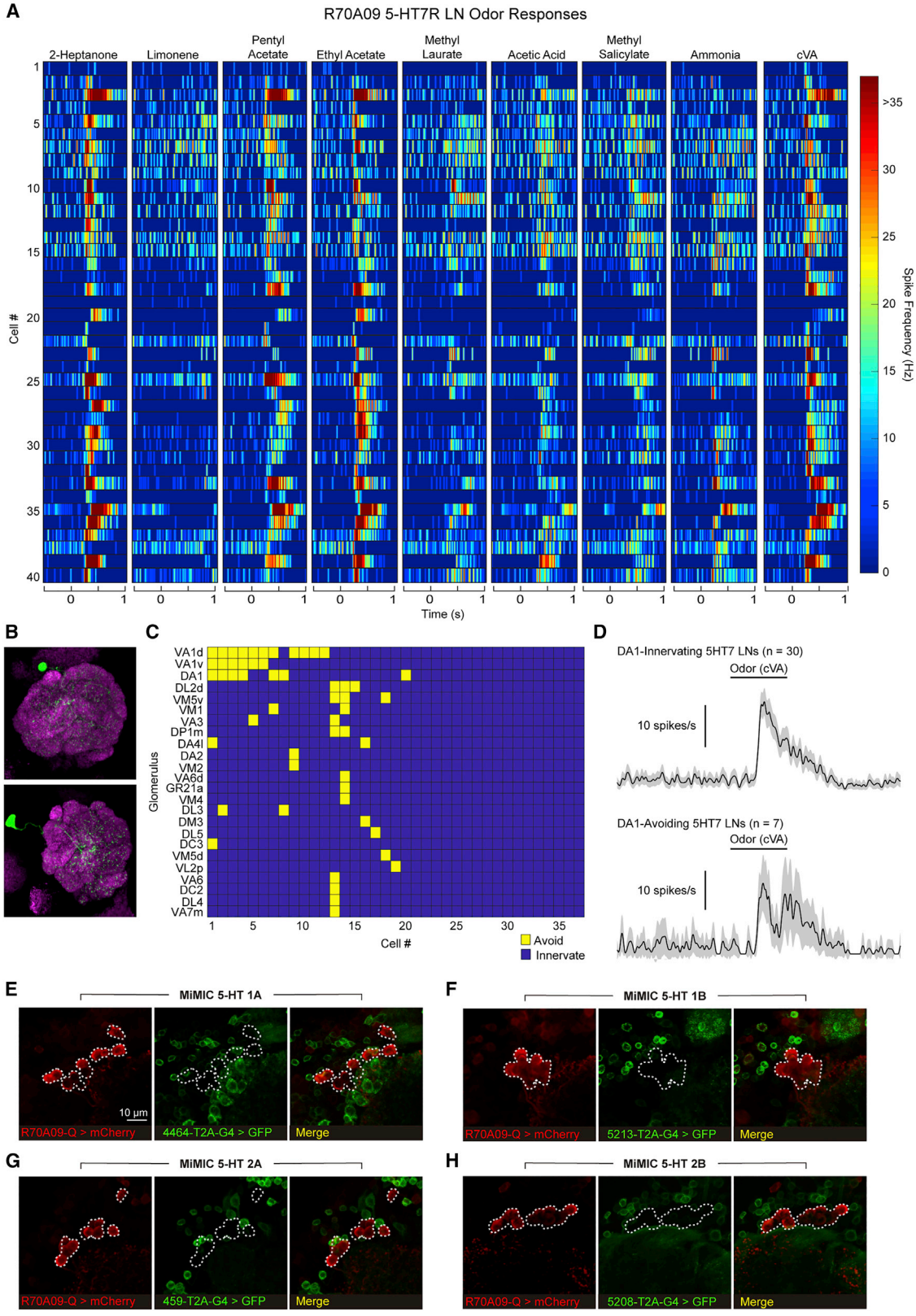

(legend on next page)

have opposing effects at high and low concentrations in the AL [8] (Figure S1), we next applied a high concentration of exogenous 5-HT to determine whether 5-HT7Rs in R70A09 LNs also signal higher serotonin concentrations. DA1 odor responses boosted to exogenous 5-HT, suggesting that 5-HT7R-expressing LNs do not signal higher concentrations of serotonin (Figures 2F–2H).

Characterization of 5-HT7R LNs

We further characterized 5-HT7R-expressing LNs with regards to their morphology, physiology, and for the expression of other 5-HTRs. The MiMIC 5-HT7R promoter line labels 11 to 12 GABAergic LNs [12]. We performed whole-cell electrophysiology on 40 LNs labeled by MiMIC 5-HT7R and filled 37 of these cells to maximize our chances of recording from all 12 neurons (should each cell be a uniquely identifiable LN; Figure 3A). All of the LNs were either pan-glomerular or nearly pan-glomerular [15], with pheromone-sensing glomeruli, such as DA1 and VA1d, being the most commonly avoided (Figures 3B and 3C). The LNs generally responded to cVA, regardless of whether or not they innervated the DA1 glomerulus (Figures 3A and 3D). As a population, 5-HT7R LNs responded broadly to a panel of nine odorants with a range of odor response amplitudes and onset latency. We used the R70A09-Q promoter line to examine the overlap of 5-HT7-expressing LNs with the well-characterized NP3056-Gal4 and GH298-Gal4 LN lines [15]. We found little overlap between any of these lines, suggesting that 5-HT7R-expressing LNs are a relatively distinct population of LNs (Figures S3D and S3E). Finally, we examined the overlap between 5-HT7R-expressing R70A09-Q LNs and the MiMIC 5-HTR lines for the additional four 5-HTRs. We found no overlap in the AL between these lines, suggesting that there exists a population of LNs that exclusively expresses the 5-HT7 receptor that partly mediates the suppressive effects of low 5-HT concentrations (Figures 3E–3H).

5-HT7R-Expressing LNs Mediate Gain Control via Postsynaptic GABAergic Transmission

Modulation of 5-HT7R-expressing LNs could suppress odor responses by either presynaptically inhibiting ORNs or postsynaptically targeting PNs. The best described role for GABAergic LNs in the AL is to mediate gain control by presynaptically targeting ORNs [19–21]. Interestingly, we found that methysergide had no effect on DA1 ORN output as measured via GCaMP [22] (Figures 4A and 4B). We have previously shown that odor responses of multiple PN classes, including DM6 and DM1, are also boosted and suppressed by methysergide and fluoxetine, respectively [8]. Neither the cognate ORNs for DM6 (OR67a) or DM1 (OR42b) were affected by methysergide application (Figures 4C and 4D), suggesting that modulation at those glomeruli is also postsynaptic and that our results generalize to non-pheromone-sensing glomeruli in the AL. Consistent with our whole-cell recordings, methysergide did boost DA1 PN odor responses measured with GCaMP (Figures 4E and 4F), suggesting that 5-HT7R LNs do likely target postsynaptic PNs.

To demonstrate a connection between 5-HT7R LNs and DA1 PNs, we expressed channelrhodopsin (Chrimson) [23] in R70A09 LNs while recording from DA1 PNs. Stimulation of these LNs reliably inhibited PNs (Figure 4G). However, as LNs in the *Drosophila* AL can be highly interconnected [24], this effect could be polysynaptic. We used our recently developed TERPS technique [8, 25] to isolate a direct, monosynaptic connection. We co-expressed Chrimson along with the TTX-insensitive sodium channel NaChBac [26, 27] in the LNs and recorded from DA1 PNs (Figure 4H). TTX was then applied to block non-NaChBac-mediated spikes and eliminate all polysynaptic connections. The inhibitory synapse between R70A09 LNs and DA1 PNs is likely monosynaptic and GABAergic, as it remains even after the application of TTX and because it is sensitive to GABA pharmacology (Figures 4I and 4J). We repeated this experiment on randomly sampled PNs to demonstrate that such connections are not specific to the DA1 glomerulus. Here, we applied the $GABA_A$ and $GABA_B$ antagonists sequentially and found that most of the inhibition is mediated via $GABA_B$ receptors (Figure 4K). To complement our TERPS approach, we expressed an RNAi targeting the $GABA_B$ receptor [20] specifically in DA1 PNs and found RNAi expression prevented methysergide's ability to boost PN odor responses (Figure 4L). Together, these data suggest a direct monosynaptic connection between 5-HT7R-expressing LNs and DA1 PNs. However, these results do not expressly rule out potential contributions from polysynaptic connections in addition to the monosynaptic connection.

Although presynaptic gain control has been well described in the AL [19, 20], comparatively little is known about postsynaptic

Figure 3. Characterization of MiMIC 5-HT7 LNs

(A) Responses of 40 recorded MiMIC 5-HT7 LNs to a panel of nine odors. Recordings were made with whole-cell patch-clamp electrophysiology. Each odor was presented for 0.5 s at time 0. Spike frequencies shown are mean frequencies taken over 50-ms intervals. Some recordings exceeded the maximum frequency represented (37.003 Hz). However, these spike rates are in the 99th percentile observed within this dataset. Therefore, all frequencies observed above the 99th percentile are represented as the same frequency as the cutoff value (37.003 Hz) to better illustrate more common, weaker responses. All odors were presented at a 1,000-fold dilution except cVA, which was diluted 10-fold.

(B) Example morphologies of 5-HT7 LNs generated via cell fills during electrophysiological recordings. Commonly observed morphologies included pan-glomerular (top) and nearly pan-glomerular (bottom).

(C) Innervation patterns for 38 cells filled during recordings in (A). Yellow indicates a glomerulus that was avoided by a given cell and blue indicates innervation. All other glomeruli not listed were innervated by every cell.

(D) PSTHs for cVA responses of cells that either innervate (top) or avoid (bottom) the DA1 glomerulus. Mean spike frequency is shown ± SEM (shaded regions). Horizontal bars indicate the 0.5-s time frame cVA was presented. Vertical bars represent spike frequency (Hz).

(E) (Left) The R70A09-Q promotor line expresses mCherry-labeling LNs on the lateral aspect of the AL. (Middle) The MiMIC-5-HT1A-Gal4 promoter line is labeled with mcd8-GFP in the same preparation. (Right) A merge of the two previous panels shows no overlap in expression. White outlines demarcate R70A09 LNs. The same scale is used in (F–H).

(F) As in (E) above but showing the lack of overlap between R70A09 LNs and MiMIC 5-HT1B neurons.

(G) As in (E) above but showing the lack of overlap between R70A09 LNs and MiMIC 5-HT2A neurons.

(H) As in (E) above but showing the lack of overlap between R70A09 LNs and MiMIC 5-HT2B neurons.

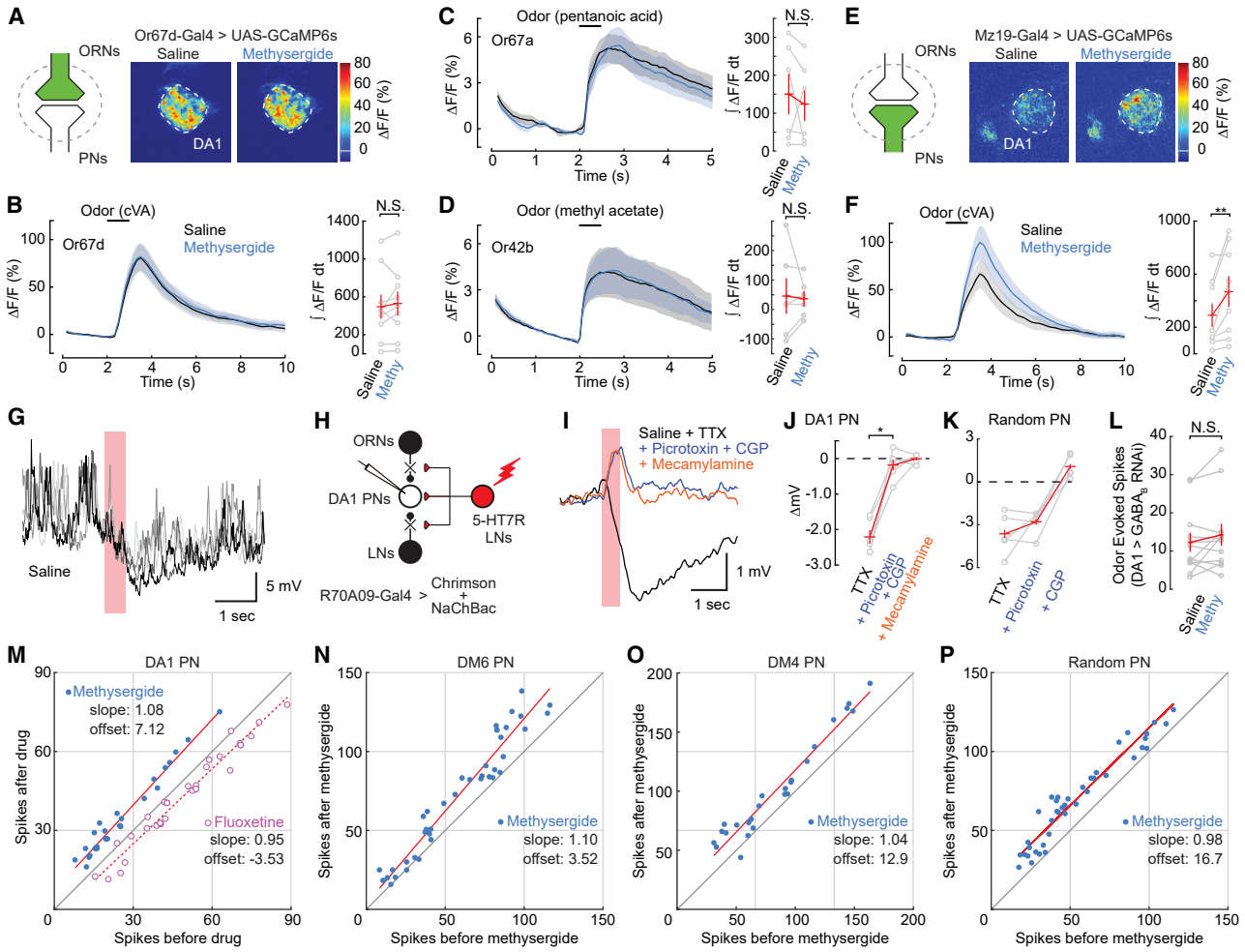

Figure 4. R70A09 LNs Use GABA to Postsynaptically Inhibit PNs

(A) Olfactory responses were assessed presynaptically via expressing GCaMP6s in the DA1 cognate ORNs, OR67d. Experiments were performed with 2-photon microscopy.

(B) Blocking basal levels of 5-HT with methysergide had no effect on OR67d odor responses. n = 9; Wilcoxon signed-rank test (p = 0.426). Odor pulse duration is 1 s. Shaded region in traces and vertical lines in summary plots represent the SEM of responses for this and subsequent panels.

(C and D) An identical protocol was used as in (B) but for Or67a- and Or42b-expressing ORNs, respectively. ORNs were stimulated with their preferred odorants depicted above the calcium responses. Experiments were performed with wide-field imaging. Or67a; n = 6; Wilcoxon signed-rank test; p = 0.31. Or42b; n = 6; Wilcoxon signed-rank test; p = 0.84.

(E) PN odor responses were assessed with 2-photon microscopy and GCaMP6s in DA1 PNs.

(F) Methysergide boosted PN responses. n = 8; Wilcoxon signed-rank test (p = 0.008).

(G) Whole-cell recordings from DA1 PNs with R70A09 LNs expressing Chrimson. DA1 PNs show hyperpolarization when R70A09 LNs were stimulated (shown in red). Each trace indicates different trials.

(H) TERPS analysis was used to determine whether the connection is monosynaptic. Chrimson and NaChBac were expressed in R70A09 LNs, and TTX was applied to block all polysynaptic connections. LNs were activated with red light and NaChBac-mediated action potentials support synaptic release. Monosynaptic responses were measured in DA1 PNs via whole-cell recording.

(I) Activating R70A09 LNs results in PN hyperpolarization that is blocked by GABAergic pharmacology.

(J) Quantification of the previous experiments. n = 5; Wilcoxon signed-rank test; p = 0.031.

(K) TERPS was performed between R70A09 LNs and randomly sampled PNs. Picrotoxin did not significantly reduce the amplitude of the synaptic inhibitory postsynaptic potential (IPSP) n = 4; Student's t test; p = 0.29. Application of CGP54626 significantly decreased amplitude of the IPSP; n = 4; Student's t test; $p < 0.001$.

(L) Expression of $GABA_B$ RNAi in DA1 PNs blocks methysergide's ability to boost odor responses to cVA. n = 12; Wilcoxon signed-rank test; p = 0.27.

(M–O) Unity plots comparing the firing rates of PNs in glomeruli DA1, DM6, and DM1 to their preferred odorants before and after pharmacological manipulations of 5-HT signaling. Points above the unity line show a boosting of odor responses after drug application. PN responses were tested at 5 different odor strengths. Additive/subtractive gain will result in an upward or downward shift of the data respective to the unity line. Red lines represent the best-fit lines to all PN data in that condition. DA1 methy n = 5; DA1 fluox n = 6; DM6 methy n = 8; DM4 methy n = 5. See also Figure S4.

(P) As in (M)–(O) but for randomly sampled PNs. The odor presented was pentyl acetate, which broadly activates ORs. n = 8.

inhibition in *Drosophila* PNs. We recorded DA1 PN responses across a broad range of cVA intensities to examine how 5-HT7 signaling mediates gain control (Figures S4A–S4C). The application of methysergide boosted both weak and strong odor responses nearly equally, suggesting the drug had at least a partial additive effect on the gain of PN output. Fluoxetine had the opposite effect and suppressed DA1 odor-evoked activity in a subtractive manner (Figure 4M). Methysergide also boosted DM6 and DM4 PN responses to odors fairly selective to their cognate ORs (Figures 4N and 4O), suggesting a conserved role for 5-HT7 signaling across the AL. Finally, we used an odorant (pentyl acetate) that broadly activates *Drosophila* ORNs [28] and sampled random PNs in the AL to determine how the global representation of odors is affected by blocking 5-HT7 signaling. The application of methysergide boosted the responses of each sampled PN across all intensities (Figure 4P).

DISCUSSION

Cellular Detection of Basal Concentrations of 5-HT

We identified a subset of GABAergic LNs that are responsible for signaling low levels of 5-HT in the AL. The 5-HT7R is well suited for detecting changes in basal concentrations of 5-HT, as it is the highest affinity serotonin receptor in *Drosophila* [29]. Interestingly, 5-HT7R-expressing LNs in the R70A09 promoter line do not appear to express any other 5-HTRs, thus suggesting they may be dedicated cellular sensors of low 5-HT levels. LNs are an ideal target for modulation as they influence several aspects of olfactory coding in both flies [30, 31] and mice [32, 33]. Serotonin is also a potent modulator of GABAergic transmission in vertebrates [34], and 5-HT targets local interneurons in the olfactory bulb (OB) as well [6, 35, 36]. LNs expressing 5-HT7R are non-specific in their glomerular innervation patterns and odor responses, suggesting a general role for their modulation. Indeed, we observed that manipulations of basal levels of serotonin signaling had similar effects across glomeruli encoding pheromones, private odors, and broadly activating public odors. However, it is critical to note 5-HT7R expression likely differs across glomeruli. We demonstrated that DA1 PNs do not express 5-HT7R, but other PNs likely do. Multiple cell classes in the AL express 5-HT7R [12] and may do so in a glomerulus-specific manner. Thus, it is likely the exact effect of 5-HT differs slightly across glomeruli and is dependent on the unique expression pattern of 5-HT7R across cell types within each glomerulus. Glomerular-specific effects of 5-HT have been reported previously [5]. Importantly, data regarding expression patterns of 5-HT7R come from approaches that label neurons according to promoters for these receptors [11, 12]. Although we can discern which cell classes express specific 5-HTRs, there are no data to verify whether individual LNs can traffic receptors to dendrites innervating specific glomeruli. Future studies employing physiology or novel molecular tools will be vital for determining how 5-HTRs are dispersed across the AL to modulate PNs innervating different glomeruli.

Postsynaptic Gain Control and Bidirectional Modulation

The best characterized form of inhibition in the AL [19, 20, 37] and OB [38, 39] is presynaptic inhibition that targets ORN terminals and mediates divisive gain control. Divisive gain control is important, as it prevents the saturation of downstream PN and mitral cell responses, allowing olfactory circuits to encode odors over a wider range of concentrations [21, 30, 40]. This form of gain control also allows the postsynaptic cell to utilize its entire dynamic range as the strength of presynaptic input increases. Finally, inhibition targeting ORNs leaves the window of temporal integration in PNs unaltered by inhibitory conductances. Interestingly, our results suggest that low-concentration 5-HT may specifically shift the balance between pre- and postsynaptic inhibition and mediate subtractive gain control. The postsynaptic inhibition arises in part from a monosynaptic connection between 5-HT7R-expressing LNs and PNs. Such direct connections from LNs onto PNs are supported by electron microscopy (EM) reconstructions of the AL in both the adult fly and larvae [24, 41]. The properties of postsynaptic inhibition are distinct from those described above [40, 42]. Postsynaptic inhibition will suppress PN firing from a broader distribution of inputs, rather than just its cognate ORNs. Subtractive gain control reduces the maximum firing rate of a neuron, thus diminishing its influence on perception, regardless of stimulus strength. This may be advantageous for suppressing behavior when sensory stimuli are presented in the wrong context. The utilization of divisive and subtractive gain control within the same circuit is not unique to olfaction, as it has also been described in the attentional regulation of vision [43].

An alternative function for the suppression by low-concentration 5-HT may be to provide stability to olfactory processing under modulation. Data from the lobster stomatogastric ganglion (STG) indicate that dopamine has opposing actions on the same neurons, depending on its concentration [44]. This mechanism has a homeostatic effect and stabilizes the motor output [45]. Similarly, we found that low and high concentrations of serotonin also have opposing effects, which are likely mediated by different receptors on different cells. Bidirectional modulation by the same transmitter has been reported in numerous other systems [46–48], suggesting it may be a common feature of the central nervous system across diverse phylogenetic groups. Indeed, as in flies, odor responses in vertebrate mitral cells are also boosted by methysergide and exogenous 5-HT [7, 35, 49]. This suggests that bidirectional modulation by 5-HT may be a universal theme in olfaction.

STAR★METHODS

Detailed methods are provided in the online version of this paper and include the following:

- KEY RESOURCES TABLE
- LEAD CONTACT AND MATERIALS AVAILABILITY
- EXPERIMENTAL MODEL AND SUBJECT DETAILS
- METHOD DETAILS
  - Odor and odor delivery
  - Whole-cell Electrophysiology
  - TERPS analysis
  - Photoactivation of caged serotonin
  - Two-photon calcium imaging
  - Single Photon Calcium Imaging
  - Pharmacology

- Cell ablation
- Immunohistochemistry

- QUANTIFICATION AND STATISTICAL ANALYSIS
- DATA AND CODE AVAILABILITY

SUPPLEMENTAL INFORMATION

Supplemental Information can be found online at https://doi.org/10.1016/j.cub.2020.01.018.

ACKNOWLEDGMENTS

This work was supported by a Whitehall Foundation grant, NIH R21 5R21DC015873-02, and NIH DC 016293 to Q.G. We would like to thank Dr. John Williams of the Vollum Institute for useful discussions regarding photo-uncaging of 5-HT and Drs. Harold Burgess and Xiaonan Zhang for critical comments on the manuscript and experimental designs. We thank A.E. Beaven and the UMD Imaging core facility for confocal imaging.

AUTHOR CONTRIBUTIONS

Y.S., J.E.S., H.T., and Q.G. all conducted experiments for this study and performed the analyses. Y.S., J.E.S., and Q.G. designed the experiments and wrote the manuscript. All authors edited the manuscript and figures.

DECLARATION OF INTERESTS

The authors declare no competing interests.

Received: March 14, 2019
Revised: September 2, 2019
Accepted: January 7, 2020
Published: March 5, 2020

REFERENCES

1. Lillesaar, C., and Gaspar, P. (2019). Serotonergic Neurons in Vertebrate and Invertebrate Model Organisms (Rodents, Zebrafish, Drosophila melanogaster, Aplysia californica, Caenorhabditis elegans) (Elsevier).
2. Schmitt, J.A., Wingen, M., Ramaekers, J.G., Evers, E.A., and Riedel, W.J. (2006). Serotonin and human cognitive performance. Curr. Pharm. Des. *12*, 2473–2486.
3. Jacobs, B.L., and Fornal, C.A. (1997). Serotonin and motor activity. Curr. Opin. Neurobiol. *7*, 820–825.
4. Jacob, S.N., and Nienborg, H. (2018). Monoaminergic neuromodulation of sensory processing. Front. Neural Circuits *12*, 51.
5. Dacks, A.M., Green, D.S., Root, C.M., Nighorn, A.J., and Wang, J.W. (2009). Serotonin modulates olfactory processing in the antennal lobe of Drosophila. J. Neurogenet. *23*, 366–377.
6. Petzold, G.C., Hagiwara, A., and Murthy, V.N. (2009). Serotonergic modulation of odor input to the mammalian olfactory bulb. Nat. Neurosci. *12*, 784–791.
7. Gaudry, Q. (2018). Serotonergic modulation of olfaction in rodents and insects. Yale J. Biol. Med. *91*, 23–32.
8. Zhang, X., and Gaudry, Q. (2016). Functional integration of a serotonergic neuron in the Drosophila antennal lobe. eLife *5*, 2435.
9. Sun, X.J., Tolbert, L.P., and Hildebrand, J.G. (1993). Ramification pattern and ultrastructural characteristics of the serotonin-immunoreactive neuron in the antennal lobe of the moth Manduca sexta: a laser scanning confocal and electron microscopic study. J. Comp. Neurol. *338*, 5–16.
10. Dacks, A.M., Christensen, T.A., and Hildebrand, J.G. (2006). Phylogeny of a serotonin-immunoreactive neuron in the primary olfactory center of the insect brain. J. Comp. Neurol. *498*, 727–746.
11. Gnerer, J.P., Venken, K.J.T., and Dierick, H.A. (2015). Gene-specific cell labeling using MiMIC transposons. Nucleic Acids Res. *43*, e56.
12. Sizemore, T.R., and Dacks, A.M. (2016). Serotonergic modulation differentially targets distinct network elements within the antennal lobe of Drosophila melanogaster. Sci. Rep. *6*, 37119.
13. Ito, K., Suzuki, K., Estes, P., Ramaswami, M., Yamamoto, D., and Strausfeld, N.J. (1998). The organization of extrinsic neurons and their implications in the functional roles of the mushroom bodies in Drosophila melanogaster Meigen. Learn. Mem. *5*, 52–77.
14. Jefferis, G.S., Vyas, R.M., Berdnik, D., Ramaekers, A., Stocker, R.F., Tanaka, N.K., Ito, K., and Luo, L. (2004). Developmental origin of wiring specificity in the olfactory system of Drosophila. Development *131*, 117–130.
15. Chou, Y.-H., Spletter, M.L., Yaksi, E., Leong, J.C.S., Wilson, R.I., and Luo, L. (2010). Diversity and wiring variability of olfactory local interneurons in the Drosophila antennal lobe. Nat. Neurosci. *13*, 439–449.
16. Jenett, A., Rubin, G.M., Ngo, T.-T.B., Shepherd, D., Murphy, C., Dionne, H., Pfeiffer, B.D., Cavallaro, A., Hall, D., Jeter, J., et al. (2012). A GAL4-driver line resource for Drosophila neurobiology. Cell Rep. *2*, 991–1001.
17. Potter, C.J., Tasic, B., Russler, E.V., Liang, L., and Luo, L. (2010). The Q system: a repressible binary system for transgene expression, lineage tracing, and mosaic analysis. Cell *141*, 536–548.
18. Lin, C.-C., and Potter, C.J. (2016). Editing transgenic DNA components by inducible gene replacement in Drosophila melanogaster. Genetics *203*, 1613–1628.
19. Olsen, S.R., and Wilson, R.I. (2008). Lateral presynaptic inhibition mediates gain control in an olfactory circuit. Nature *452*, 956–960.
20. Root, C.M., Masuyama, K., Green, D.S., Enell, L.E., Nässel, D.R., Lee, C.-H., and Wang, J.W. (2008). A presynaptic gain control mechanism fine-tunes olfactory behavior. Neuron *59*, 311–321.
21. Hong, E.J., and Wilson, R.I. (2013). Olfactory neuroscience: normalization is the norm. Curr. Biol. *23*, R1091–R1093.
22. Tian, L., Hires, S.A., Mao, T., Huber, D., Chiappe, M.E., Chalasani, S.H., Petreanu, L., Akerboom, J., McKinney, S.A., Schreiter, E.R., et al. (2009). Imaging neural activity in worms, flies and mice with improved GCaMP calcium indicators. Nat. Methods *6*, 875–881.
23. Klapoetke, N.C., Murata, Y., Kim, S.S., Pulver, S.R., Birdsey-Benson, A., Cho, Y.K., Morimoto, T.K., Chuong, A.S., Carpenter, E.J., Tian, Z., et al. (2014). Independent optical excitation of distinct neural populations. Nat. Methods *11*, 338–346.
24. Horne, J.A., Langille, C., McLin, S., Wiederman, M., Lu, Z., Xu, C.S., Plaza, S.M., Scheffer, L.K., Hess, H.F., and Meinertzhagen, I.A. (2018). A resource for the *Drosophila* antennal lobe provided by the connectome of glomerulus VA1v. eLife *7*, 1–24.
25. Zhang, X., and Gaudry, Q. (2018). Examining monosynaptic connections in Drosophila using tetrodotoxin-resistant sodium channels. J. Vis. Exp. 57052.
26. Ren, D., Navarro, B., Xu, H., Yue, L., Shi, Q., and Clapham, D.E. (2001). A prokaryotic voltage-gated sodium channel. Science *294*, 2372–2375.
27. Nitabach, M.N., Wu, Y., Sheeba, V., Lemon, W.C., Strumbos, J., Zelensky, P.K., White, B.H., and Holmes, T.C. (2006). Electrical hyperexcitation of lateral ventral pacemaker neurons desynchronizes downstream circadian oscillators in the fly circadian circuit and induces multiple behavioral periods. J. Neurosci. *26*, 479–489.
28. Hallem, E.A., and Carlson, J.R. (2006). Coding of odors by a receptor repertoire. Cell *125*, 143–160.
29. Gasque, G., Conway, S., Huang, J., Rao, Y., and Vosshall, L.B. (2013). Small molecule drug screening in Drosophila identifies the 5HT2A receptor as a feeding modulation target. Sci. Rep. *3*, p02120.
30. Wilson, R.I. (2013). Early olfactory processing in Drosophila: mechanisms and principles. Annu. Rev. Neurosci. *36*, 217–241.
31. Gaudry, Q., and Schenk, J. (2018). Drosophila olfaction. In Oxford Research Encyclopedias Neuroscience. https://oxfordre.com/neuroscience/abstract/10.1093/acrefore/9780190264086.001.0001/acrefore-9780190264086-e-167.

32. Lledo, P.-M., Saghatelyan, A., and Lemasson, M. (2004). Inhibitory interneurons in the olfactory bulb: from development to function. Neuroscientist *10*, 292–303.

33. Lledo, P.-M., Merkle, F.T., and Alvarez-Buylla, A. (2008). Origin and function of olfactory bulb interneuron diversity. Trends Neurosci. *31*, 392–400.

34. Ciranna, L. (2006). Serotonin as a modulator of glutamate- and GABA-mediated neurotransmission: implications in physiological functions and in pathology. Curr. Neuropharmacol. *4*, 101–114.

35. Brill, J., Shao, Z., Puche, A.C., Wachowiak, M., and Shipley, M.T. (2016). Serotonin increases synaptic activity in olfactory bulb glomeruli. J. Neurophysiol. *115*, 1208–1219.

36. Brunert, D., Tsuno, Y., Rothermel, M., Shipley, M.T., and Wachowiak, M. (2016). Cell-type-specific modulation of sensory responses in olfactory bulb circuits by serotonergic projections from the Raphe nuclei. J. Neurosci. *36*, 6820–6835.

37. Olsen, S.R., Bhandawat, V., and Wilson, R.I. (2010). Divisive normalization in olfactory population codes. Neuron *66*, 287–299.

38. Wachowiak, M., McGann, J.P., Heyward, P.M., Shao, Z., Puche, A.C., and Shipley, M.T. (2005). Inhibition [corrected] of olfactory receptor neuron input to olfactory bulb glomeruli mediated by suppression of presynaptic calcium influx. J. Neurophysiol. *94*, 2700–2712.

39. McGann, J.P. (2013). Presynaptic inhibition of olfactory sensory neurons: new mechanisms and potential functions. Chem. Senses *38*, 459–474.

40. Silver, R.A. (2010). Neuronal arithmetic. Nat. Rev. Neurosci. *11*, 474–489.

41. Berck, M.E., Khandelwal, A., Claus, L., Hernandez-Nunez, L., Si, G., Tabone, C.J., Li, F., Truman, J.W., Fetter, R.D., Louis, M., et al. (2016). The wiring diagram of a glomerular olfactory system. eLife *5*, 450.

42. Holt, G.R., and Koch, C. (1997). Shunting inhibition does not have a divisive effect on firing rates. Neural Comput. *9*, 1001–1013.

43. Reynolds, J.H., and Heeger, D.J. (2009). The normalization model of attention. Neuron *61*, 168–185.

44. Rodgers, E.W., Fu, J.J., Krenz, W.D.C., and Baro, D.J. (2011). Tonic nanomolar dopamine enables an activity-dependent phase recovery mechanism that persistently alters the maximal conductance of the hyperpolarization-activated current in a rhythmically active neuron. J. Neurosci. *31*, 16387–16397.

45. Harris-Warrick, R.M., and Johnson, B.R. (2010). Checks and balances in neuromodulation. Front. Behav. Neurosci. *4*, 1–9.

46. Teshiba, T., Shamsian, A., Yashar, B., Yeh, S.R., Edwards, D.H., and Krasne, F.B. (2001). Dual and opposing modulatory effects of serotonin on crayfish lateral giant escape command neurons. J. Neurosci. *21*, 4523–4529.

47. Nai, Q., Dong, H.-W., Hayar, A., Linster, C., and Ennis, M. (2009). Noradrenergic regulation of GABAergic inhibition of main olfactory bulb mitral cells varies as a function of concentration and receptor subtype. J. Neurophysiol. *101*, 2472–2484.

48. Nai, Q., Dong, H.W., Linster, C., and Ennis, M. (2010). Activation of alpha1 and alpha2 noradrenergic receptors exert opposing effects on excitability of main olfactory bulb granule cells. Neuroscience *169*, 882–892.

49. Kapoor, V., Provost, A.C., Agarwal, P., and Murthy, V.N. (2016). Activation of raphe nuclei triggers rapid and distinct effects on parallel olfactory bulb output channels. Nat. Neurosci. *19*, 271–282.

50. Jeanne, J.M., and Wilson, R.I. (2015). Convergence, divergence, and reconvergence in a feedforward network improves neural speed and accuracy. Neuron *88*, 1014–1026.

51. Dana, H., Sun, Y., Mohar, B., Hulse, B.K., Kerlin, A.M., Hasseman, J.P., Tsegaye, G., Tsang, A., Wong, A., Patel, R., et al. (2019). High-performance calcium sensors for imaging activity in neuronal populations and microcompartments. Nat. Methods *16*, 649–657.

STAR★METHODS

KEY RESOURCES TABLE

REAGENT or RESOURCE	SOURCE	IDENTIFIER
Antibodies		
nc82 Antibody Supernatant 1.0 mL	Developemental Studies Hybridoma Bank	Cat# nc82; RRID: AB_2314866
CD8a Rat Anti-Mouse mAb (clone 5H10), Unconjugated	Life Technologies	Cat# MCD0800; RRID: AB_467087
Anti-Serotonin antibody produced in rabbit	Sigma-Aldrich	Cat# S5545-.2ml; RRID: AB_477522
Living Colors® DsRed Polyclonal Antibody	Clontech	Cat# 632496; RRID: AB_10013483
Alexa Fluor® 568 Goat Anti-Mouse IgG (H+L) Antibody	Life Technologies	Cat# A-11004; RRID: AB_2534072
Alexa Fluor® 488 Goat Anti-Rat IgG (H+L) Antibody	Life Technologies	Cat# A-11006; RRID: AB_2534074
Alexa Fluor® 633 Goat Anti-Rabbit IgG (H+L), highly cross-adsorbed	Life Technologies	Cat# A-21071; RRID: AB_2535732
streptavidin, Alexa Fluor® 568 conjugate	Invitrogen	Cat# S11226; RRID: AB_2315774
Biocytin Hydrazide	Life Technologies	Cat# B-1603
Chemicals, Peptides, and Recombinant Proteins		
Paraffin oil	J.T.Baker	CAS: 8012-95-1
11-cis-Vaccenyl acetate	Pherobank, Wijk bij Duurstede, Netherlands	CAS: 6186-98-7
Pentyl acetate	Sigma-Aldrich	CAS: 628-63-7
Pentanoic acid (valeric acid)	Sigma-Aldrich	CAS: 109-52-4
Methyl acetate	Sigma-Aldrich	CAS: 79-20-9
2-Heptanone	Sigma-Aldrich	CAS: 110-43-0
Limonene	Sigma-Aldrich	CAS: 5989-27-5
Ethyl Acetate	Sigma-Aldrich	CAS: 141-78-6
Methyl Laurate	Sigma-Aldrich	CAS: 111-82-0
Acetic Acid	Sigma-Aldrich	CAS: 64-19-7
Methyl Salicylate	Sigma-Aldrich	CAS: 119-36-8
Ammonia	Sigma-Aldrich	CAS: 1336-21-6
WAY100635	Tocris	CAS: 634908-75-1
SB216641	Tocris	CAS: 193611-67-5
Ketanserin	Tocris	CAS: 83846-83-7
Metoclopramide	Sigma-Aldrich	CAS: 364-62-5
SB258719	Tocris	CAS: 1217674-10-6
Methysergide	Tocris	CAS: 129-49-7
Fluoxetine	Tocris	CAS: 56296-78-7
Tetrodotoxin	Tocris	CAS: 18660-81-6
Mecamylamine	Sigma-Aldrich	CAS: 826-39-1
Picrotoxin	Sigma-Aldrich	CAS: 124-87-8
NPEC-caged-serotonin	Tocris	CAS: 1257326-22-9)
CGP54626	Tocris	CAS: 149184-21-4
Serotonin	Sigma-Aldrich	CAS: 153-98-0
Experimental Models: Organisms/Strains		
QF-Mz19	Bloomington	RRID:BDSC_41573
QUAS-mCD8::GFP	Bloomington	RRID:BDSC_30002
Gal4-Mz19	Bloomington	RRID:BDSC_34497
Gal4-GH298	Bloomington	RRID:BDSC_37294
UAS-5-HT7 RNAi	Bloomington	RRID:BDSC_32471
Gal4-NP3056	DGRC	RRID:113080

(*Continued on next page*)

Continued

REAGENT or RESOURCE	SOURCE	IDENTIFIER
Gal4-GMR70A09	Bloomington	RRID:BDSC_47720
20 × UAS-IVS-mCD8::GFP	Bloomington	RRID:BDSC_32194
10 × QUAS-6 × mCherry	Bloomington	RRID:BDSC_52269
UAS-GFP.nls	Bloomington	RRID:BDSC_4776
10 × UAS-IVS-mCD8::GFP	Bloomington	RRID:BDSC_32194
Or67d-Gal4	Bloomington	RRID:BDSC_23906
Or42b-Gal4	Bloomington	RRID:BDSC_9971
20 × UAS-IVS-chrimson	Bloomington	RRID:BDSC_55135
UAS-NaChBac	Bloomington	RRID:BDSC_9469
Gal4-NP3062	DGRC	RRID:113083
UAS-Dipth^{ts}	Bloomington	RRID:BDSC_25039
w^{1118}	Bloomington	RRID:BDSC_5905
Gal4-GMR60F02	Bloomington	RRID:BDSC_48228
Gal4-Trh	Bloomington	RRID:BDSC_38389
UAS-VMAT-RNAi	Bloomington	RRID:BDSC_44471
Or83b-QF2^{G4H}	Bloomington	RRID:BDSC_26818
QUAS-FLP	Bloomington	RRID:BDSC_30127
10 × UAS-(FRT.stop)GFP	Bloomington	RRID:BDSC_55810
10 × QUAS-6 × GFP	Bloomington	RRID:BDSC_52264
10 × UAS-RFP	Bloomington	RRID:BDSC_32219
Mi{MIC}5-HT1A-T2A-Gal4^{MI01140}	Herman Dierick	N/A
Mi{MIC}5-HT1A-T2A-Gal4^{MI04468}	Herman Dierick	N/A
Mi{MIC}5-HT1A-T2A-Gal4^{MI04464}	Herman Dierick	N/A
Mi{MIC}5-HT1B-T2A-Gal4^{MI05213}	Herman Dierick	N/A
Mi{MIC}5-HT2A-T2A-Gal4^{MI00459}	Herman Dierick	N/A
Mi{MIC}5-HT2A-Gal4^{MI03299}	Herman Dierick	N/A
Mi{MIC}5-HT2B-T2A-Gal4^{MI05208}	Herman Dierick	N/A
Mi{MIC}5-HT2B-T2A-Gal4^{MI06500}	Herman Dierick	N/A
Mi{MIC}5-HT7-Gal4^{MI00215}	Herman Dierick	N/A
UAS-GABAB-RNAi; UAS-GABAB-RNAi	Jing Wang	N/A
UAS-5-HT7	Julian Dow	N/A
GMR70A09-QF2^{G4H}	Generated in this study	N/A
Or67d-Gal4	Bloomington	RRID:BDSC_23906
20 × UAS-IVS-GCaMP6s	Bloomington	RRID:BDSC_42746

LEAD CONTACT AND MATERIALS AVAILABILITY

Further information and requests for resources and reagents should be directed to and will be fulfilled by the Lead Contact, Quentin Gaudry (qgaudry@umd.edu). All unique/stable reagents generated in this study are available from the Lead Contact without restriction.

EXPERIMENTAL MODEL AND SUBJECT DETAILS

Flies were reared on Nutri-Fly Bloomington Formulation (Flystuff.com, San Diego, CA) at 25°C in 1-pint plastic bottles. All experiments were performed on female flies 1–3 days post-eclosion. All fly stocks containing the optogenetic transgene Chrimson [23] were raised on rehydrated potato flakes (Carolina Biological, Burlington, NC) mixed with 0.2 mM all-trans-retinal.

METHOD DETAILS

Odor and odor delivery

Odors were presented as previously described [8]. In brief, a carrier stream of carbon-filtered house air was continuously presented at 2.2 L/min to the fly. A solenoid was used to redirect 200 ml/min of this air stream into an odor vial before rejoining the carrier stream,

thus diluting the odor a further 10-fold prior to reaching the animal. cVA (Pherobank, Wageningen, Netherlands) was delivered as a pure odorant before the 10-fold carrier stream dilution. For all experiments, the odor was presented every 40 s. In Figure 4, we varied the odor strength by adding a solenoid valve between the odor vial and the carrier tube [50]. This allowed us to flush the odor vial before redirecting the odor to the fly. Flushing the odor vial for longer time periods resulted in lower effective concentrations of the odor at the fly. We verified this olfactometer with a photo-ionization device (Aurora Scientific, Ontario Canada, mini-PID 200B) as seen in Figure S4.

Whole-cell Electrophysiology

In vivo whole-cell recordings were performed as previously described [8]. Data were low-pass filtered at 5 kHz using an AM Systems model 2400 amplifier (AM Systems, Carlsberg, Washington) and digitized at 10 kHz. Pipettes were pulled from thin-walled borosilicate glass (World Precision Instruments, Sarasota, FL; 1.5 mm outer diameter, 1.12 mm inner diameter) to a resistance of 8–12 MΩ. To visualize neurons, we used oblique illumination from an infrared LED guided through a fiber optic (Thorlabs, Newton, New Jersey). The external recording solution contained, (in mM) 103 NaCl, 3 KCl, 5 N-tris(hydroxymethyl)methyl-2-aminoethane-sulfonic acid, 8 trehalose, 10 glucose, 26 NaHCO3, 1 NaH2PO4, 1.5 CaCl2, and 4 MgCl2 (adjusted to 270–275 mOsm). The saline was bubbled with 95% O_2/5% CO_2 and reached a pH of 7.3. Our internal solution contained, (in mM) 140 potassium aspartate, 10 HEPES, 4 MgATP, 0.5 Na3GTP, 1 EGTA, and 1 KCl. Cells recorded for Figure 3 were filled with biocytin in the internal solution for post hoc morphology visualization via confocal microscopy. For whole cell recordings, a small hyperpolarizing current was applied to offset the depolarization caused by the pipette seal conductance. The cells' resting potentials were adjusted slightly to match the firing rate of similar neurons obtained in cell-attached recordings. Neurons which did not fire spontaneously or that had depolarized membrane potentials upon break-in were excluded from the study. DA1 PNs were labeled using the Q/QUAS system [17] with the MZ19-QF promoter. These cells were identified based on their soma location in the lateral cluster of the antennal lobe and responsiveness to cVA.

GABAergic LNs in the MiMIC-5-HT7R promoter line were targeted based on soma size and location. The cells were labeled using nuclear localized GFP (nls-GFP) to reduce the total fluorescence in the preparation. We believe we did not record from glutamatergic LNs as their cell bodies are located in the ventral AL and they have distinct physiology that differentiates them from GABAergic LNs. Uniglomerular PNs and GABAergic PNs were excluded from our analyses based on morphology revealed by neurobiotin. All flies used in the MiMIC-5-HT7R promoter line were heterozygous for both transgenes and only female flies were utilized.

The CSDns in Figure S4 were activated via Chrimson activation with a 10Hz sinewave of 660nm red light. Activation proceeded during all of the inter trial intervals for those preparations and stopped while odor responses were collected.

TERPS analysis

We expressed NaChBac and Chrimson in LNs with the GMR70A09-Gal4 line. This promoter line labels LNs and only a small set of additional neurons outside the AL. TTX (1 μM) was used to block all spiking in the AL. We confirmed this by depolarizing each neuron and observing they could no longer fire action potentials. We used a high-powered red LED (Red XP-E, 620-630 nm wavelength) and Buckpuck driver (RapidLED, Randolph, Vermont) to stimulate GMR70A09 neurons expressing Chrimson and NaChBac. The LED was mounted directly underneath the preparation and light was presented at 0.238 mW/mm^2 as measured by a Thorlabs light meter PM100A with light sensor S130C. LED activation would result in a hyperpolarization in the postsynaptic cell. Once TTX was added, the duration of the LED pulse was adjusted to ensure that the hyperpolarization persisted. This duration varied from 100 ms to 500 ms across preparations but was kept constant for each fly. GABA antagonists were then added to the recirculating perfusion system to determine the nature of the chemical synapse. As with previous studies [8], we found a depolarizing response which remained even in the presence of the acetylcholine antagonist mecamylamine. This depolarization is presumed to be mediated by gap junctions as it is insensitive to cadmium, a non-specific calcium channel blocker that prevents synaptic transmission. Flies expressing Chrimson were raised on food containing 0.2 mM all-trans-retinal. All-trans retinal was prepared as a stock solution in ethanol (35 mM), and 28 μL of this stock was mixed into approximately 5 mL of rehydrated potato flakes and added to the top of a vial of conventional food.

Photoactivation of caged serotonin

We used a high-power UV LED (M365LP1, 365 nm wavelength, Thorlabs) to elicit photolysis of caged-serotonin. The light was presented at 0.2 mW with a 20 ms pulse. The external saline containing caged-serotonin was recirculated at the beginning of experiments, and we replaced it every experiment. To prevent undesirable photolysis, we shielded the preparation from ambient light.

Two-photon calcium imaging

Imaging was performed *in vivo* on flies using a similar approach to our electrophysiological recordings. A custom chamber was made that possessed a piece of steel foil with a hole cut out to match the perimeter of the fly's body. The fly was inserted into the foil and a small window was cut into the fly head capsule to view the brain. The glial sheathing overlying the brain remained intact. We used female flies aged 3 days post-eclosion and reared at room temperature. Imaging experiments were performed at room temperature. Flies were dissected in the same manner as those used in whole cell recordings and perfused with the same extracellular solution. The saline was bubbled with 95% O_2/5% CO_2 and reached a pH of 7.3. 920 nm wavelength light was used to excite GCaMP6s under two-photon microscopy. The microscope and data acquisition were controlled by ThorImage 3.0 (Thorlabs, Inc.). An image of the sample was scanned at a speed of 60 frames/second and averaged every 10 frames. Thus, the sample was recorded

at 6 frames/second. Odors were delivered for 1 s after the first 2 s of each trial. An inter-trial interval of 80 s was applied between each trial. A volumetric ROI was set manually for each experiment that surrounded the DA1 glomerulus. Calcium transients (ΔF/F) were measured as changes in fluorescence, in which ΔF/F was calculated by normalizing the fluorescence brightness changes over the baseline period (the first 2 s of each trial before the odor delivery).

Single Photon Calcium Imaging

We performed some of our ORN imaging experiments using wide-field single photon imaging due to its simplicity over the 2-photon approach. GCAMP7s [51] was expressed in ORNs of interest (OR67a and OR42b) using the GAL4/UAS binary expression system. Flies expressing GCAMP7s were mounted in a custom chamber identical to that employed for physiology and 2-photon imaging. The head capsule was opened, and antennal lobes were imaged using a CMOS camera (Photometrics Prime). Videos were captured at 50 Hz framerate. GCAMP7s was excited with a blue LED and shuttered between trials. Odors were delivered in 0.5 s pulses each minute via the same olfactometer used throughout the study. The labeled glomerulus was determined by eye and a focal plane of approximately the middle of the glomerulus was imaged. Ten odor presentations were recorded in external saline solution perfusion followed by ten presentations in 50 μM methysergide. Mean change in fluorescence over baseline and SEM was measured in MATLAB. Statistical difference was determined via Wilcoxon Signed Rank test.

Pharmacology

The following chemicals were used in this study at the concentrations indicated: methysergide maleate (50 μM, Tocris, CAS 129-49-7), fluoxetine (10 μM, Tocris/Sigma, CAS 56296-78-7), WAY100635 (20 μM, Tocris, CAS 634908-75-1), SB216641 (20 μM, Tocris, CAS 193611-67-5), ketanserin (20 μM, Tocris, CAS 83846-83-7), metoclopramide (20 μM, Sigma, CAS 364-62-5), SB258719 (20 μM, Tocris, CAS 1217674-10-6), CGP54626 (50 μM, Tocris, CAS 149184-21-4), mecamylamine (100 μM, Sigma, CAS 826-39-1), tetrodotoxin (TTX) (1 μM, Tocris, CAS 18660-81-6), picrotoxin (5 μM, Sigma, CAS 124-87-8), NPEC-caged-serotonin (50 μM, Tocris, CAS 1257326-22-9), and serotonin (100 μM, Sigma, CAS 153-98-0). Serotonin solutions were made fresh from powder immediately prior to each experiment and wrapped tightly in aluminum foil to prevent oxidation by light. We used a peristaltic pump to recirculate the external recording solution in all experiments using pharmaceuticals. Drugs were added sequentially to the same recirculating solution.

Cell ablation

Cell ablation by diphtheria toxin was performed as previously described [8]. In brief, a temperature-sensitive variant of diphtheria toxin was expressed in the CSDn or Trh neurons by the GAL4/UAS system. One-day post eclosion, adult flies were transferred to 31°C for three days. The efficiency of the diphtheria toxin was assessed by immunohistochemistry with the serotonin antibody for each preparation post hoc.

Immunohistochemistry

Dissected brains were fixed with 4% paraformaldehyde for 15 min at room temperature. Fixed tissue was blocked with PBS containing 2% Triton X-100 and 10% normal goat serum (NGS) for 30 min and then incubated for 1 day each (with washing in between) at room temperature in PBS containing 1% Triton X-100, 0.25% NGS, and a primary antibody or secondary antibody solution. The brain was mounted in 20 μL Vectashield medium. We used the following primary antibodies at the indicated dilutions: 1:50 mouse anti-bruchpilot (nc82) (Developmental Studies Hybridoma Bank, Iowa), 1:1000 rabbit anti-5HT (Sigma, S5545). Secondary antibodies from Invitrogen were used at dilutions of 1:250, which were Alexa Fluor 633 goat anti-mouse IgG (Life Technologies, A21050), Alexa Fluor 568 goat anti-mouse IgG (Life Technologies, A11004), Alexa Fluor 633 goat anti-rabbit (Invitrogen, A21071). Confocal images were acquired with Zeiss LMS710 confocal laser scanning microscope under 40x or 63x magnification.

QUANTIFICATION AND STATISTICAL ANALYSIS

Statistical results for each experiment can be found in the figure legents. Values are given as means ± SEM. As only one neuron was sampled per fly, n-values are reported as either a fly or a neuron. Wilcoxon signed rank tests were performed for all paired comparisons between one treatment and the control within the same group. Significance was determined by a p value less than or equal to 0.05 and sample sizes were based on similar studies in the field. For physiological measurements, these ranged from 6 – 12 animals and between 3 – 6 for qualitative immunohistochemistry. All cells which received pharmacological treatments were included in the study. If a cell had a depolarized resting membrane potential or poor access resistance, the recording was terminated before pharmacological manipulation.

DATA AND CODE AVAILABILITY

The accession number for the physiological and immunohistochemistry data reported in this paper is Zenodo: Database: https://doi.org/10.5281/zenodo.3590444.